Electronic Supplementary Material (ESI) for Journal of Materials Chemistry B.

Electronic Supplementary Information

Au nanoparticle in situ decorated RGO nanocomposites for highly sensitive electrochemical genosensors

Chiara Ingrosso[1,*], Michela Corricelli[1], Francesca Bettazzi[2], Evgenia Konstantinidou[2], Giuseppe V. Bianco[3], Nicoletta Depalo[1], Marinella Striccoli[1], Angela Agostiano[1,4], M. Lucia Curri,[1] Ilaria Palchetti[2]

[1]CNR-IPCF S. S. Bari, c/o Dep. of Chemistry, Università di Bari, via Orabona 4, I-70126 Bari, Italy
[2]Dep. of Chemistry Ugo Schiff, Università degli Studi di Firenze, via della Lastruccia 3-13, 50019 Sesto Fiorentino, Firenze, Italy
[3]CNR-NANOTEC, c/o Dep. of Chemistry, Università di Bari, via Orabona 4, I-70126, Bari, Italy
[4]Dep. of Chemistry, Università di Bari, via Orabona 4, I-70126 Bari, Italy
*Email: c.ingrosso@ba.ipcf.cnr.it

Figure S1(A) reports the TEM image of a bare RGO flake, after the *in situ* synthesis of the Au NPs, with TOAB, DMBT and $NaBH_4$.

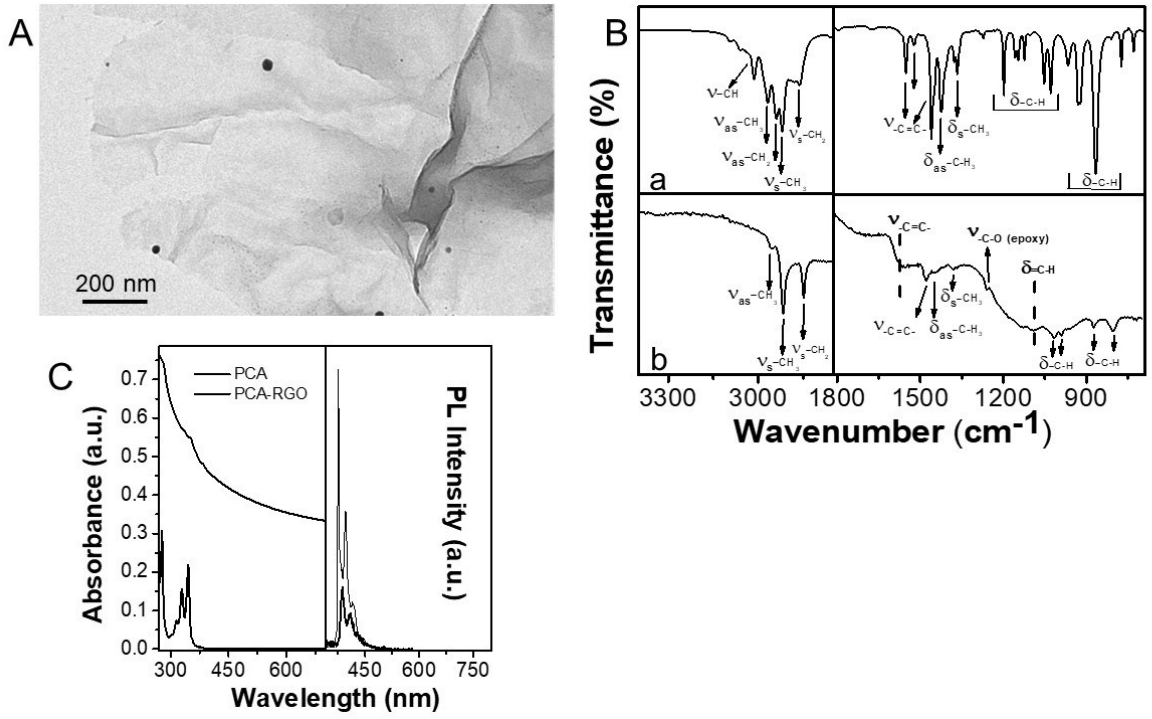

Fig. S1. (A) TEM images of RGO sheets, as bare, after the *in situ* synthesis of the Au NPs with TOAB, DMBT and $NaBH_4$. (B) FTIR-ATR spectra of (a) neat DMBT thiol and (b)

PCA-RGO/Au NPs hybrid flakes. (C) UV-Vis absorption (left panel) and PL spectra (right panel) of 10^{-9} M PCA and of 0.15 mg mL^{-1} PCA-RGO in toluene.

The micrograph of the bare RGO flakes presents only few nano-objects with an intense contrast, reasonably ascribed to Au NPs, thus suggesting the scarcity of oxygen containing functional groups at the surface of RGO, able to anchor the Au NPs, and indicating the involvement of the carboxyl groups of PCA in coordinating,[1] and hence, binding the Au NPs to the sheets surface. To further confirm the control experiment, ATR-FTIR investigation of the PCA-RGO flakes has been performed. Figure S1 (B)) reports the ATR-FTIR spectrum of the hybrid flakes, compared with that of the neat DMBT thiol. The spectrum of the PCA-RGO/Au NPs hybrid flakes shows, in the high wavenumber region, asymmetric and symmetric stretching modes of $–CH_3$ at 2954 cm^{-1} and 2917 cm^{-1}, respectively, and symmetric stretching vibrations of $–CH_2$ at 2848 cm^{-1}, which can be ascribed to the thiol coordinated to the surface of the Au NPs. Indeed, in the high wavenumber region of the spectrum, the thiol shows peaks at 3060 cm^{-1} and 3014 cm^{-1}, ascribed to the –CH stretching vibrations of the aromatic ring, at 2968 cm^{-1} and 2919 cm^{-1}, the asymmetric and symmetric stretching modes of $–CH_3$, and at 2941 cm^{-1} and 2862 cm^{-1}, the asymmetric and symmetric stretching vibrations of $–CH_2$. Conversely, in the low wavenumber region of the spectrum of the hybrid, the large bands at 1565 cm^{-1}, and between 1300 and 900 cm^{-1}, can be ascribed to the skeletal stretching and bending vibrations of the –C=C- and =C-H of the RGO aromatic platform, respectively.[2] Finally, only the peak of epoxy functionalities at 1260 cm^{-1}, residual from the reduction process of GO to RGO, also induced by $NaBH_4$ and catalyzed by the immobilized Au NPs,[3] is evident.[4] The other weak and narrow bands are mainly ascribed to the thiol molecules coordinating the NP surface. Namely, the band at 1479 cm^{-1} is due to the –C=C- aromatic stretching of the ring, those at 1447 cm^{-1} and 1379 cm^{-1} are ascribed to the bending vibrations of the peripheral $-CH_3$ groups of the ring, and those at 1015

cm^{-1}, 995 cm^{-1}, 873 cm^{-1} and 805 cm^{-1} are the bending vibrations of the aromatic –CH of the thiol. For purpose of clarity, in the infrared spectrum of the thiol, the vibrations at 1600 cm^{-1} and 1491 cm^{-1} are ascribed to the –C=C- stretching of the aromatic ring, the modes at 1449 cm^{-1} and at 1395 cm^{-1} are due to the asymmetric and symmetric bending vibrations of $–CH_3$, respectively, and the bands located at 1189, 1142, 1129 1103, 1021, 991 cm^{-1}, and those at 916, 870 and 806 cm^{-1} are explained by the in plane and out of plane bending vibrations modes of the ring, respectively.

It is worthwhile to notice that in the investigated conditions, the infrared spectrum does not account for the presence of PCA onto the RGO sheets, because the carboxylic group vibration of PCA, expected at around 1690 cm^{-1},[5] is not detectable in the recorded spectrum. Nevertheless, the effective anchoring of the pyrene ligand onto the RGO platform is confirmed both by the presence of the broad background signal in the Raman spectrum of the hybrid (panel E of Figure 1) which originates from the PCA photoluminescence,[6] and by the presence of the absorption and PL signals of PCA in the UV-Vis absorption and PL spectra of the PCA-RGO flakes (Figures S1(C)).

The absorption spectrum of the PCA-RGO complex shows an increase in the baseline intensity due to scattering phenomena originated from the PCA-RGO flakes, a featureless absorption line-shape in the visible range, as well as absorption broad signals at 329 nm and 346 nm in the near UV region, which can be ascribed to the π-π^* transitions of the –C=C– bonds, attesting for the anchoring of the pyrene ligand on the suspended sheets (left panel of Figure S1 C).[7]

Upon binding to the Au NPs, the sharp and distinct absorption bands of the PCA molecules appear as shoulders in the line-shape, and this change reflects modifications in the electronic properties of PCA upon complexation to an Au NP, arising from strong ground-state interactions between the plasmon electrons of Au NPs and the π-electron cloud of PCA (left panel of Figure S1 C).[8] In the right panel of Fig. S1 C, the PL emission spectrum of the PCA-RGO complex shows the PL peaks of PCA at 386 nm and 408 nm,[6] respectively, which are

however markedly modified in the relative peak intensities, upon formation of the PCA-RGO complex. Such an evidence can be due to a change in the chemical environment of PCA, that from being dispersed in toluene, passes to be bound to the more nonpolar RGO surface.[9]

Table S1. Electroactive area and electron transfer rate constant (k_0) of SPCE, as bare and modified by PCA-RGO/Au NPs, in 5 mM $[Fe(CN)_6]^{3-/4-}$ and 0.1 M KCl, with a geometric area of SPCE of 7 mm^2.

Electrode	A_{ele} (mm^2)	K_0 ($cm\ s^{-1}$)
Bare SPCE	9 ± 1	$2.7 \pm 0.5 \times 10^{-4}$
PCA-RGO/Au NPs SPCE	14 ± 2	$9.3 \pm 0.7 \times 10^{-4}$

Voltammetric determination of tetramethyl benzidine (TMB).

TMB is a common substrate for HRP, and the mechanism of oxidation of TMB by HRP, in presence of H_2O_2, is a well-known process. Oxidation of TMB by HRP/H_2O_2 first generates a blue-colored complex product, which turns yellow after the addition of sulfuric acid to the reaction media. This yellow product has been identified as a two-electron oxidation product, namely diimine, which is stable in acid solutions and it is electroactive. CV studies have been carried out in a neutral (Fig. S2(A)) and at an acid pH (Fig. S2(B)), wherein the enzymatic product, yellow diimine is stable. Fig. S2(B) shows the CV of the substrate mixture (TMB/H_2O_2) in 0.5 M H_2SO_4 solution; it is characterized by a well-defined redox behaviour with ΔE_p = 40 mV around the expected Nerstian value for a two electron reversible process.[10] When TMB/H_2O_2 substrate mixture is incubated in the presence of HRP prior to the addition of the stopping solution, the electrochemical oxidation of TMB is accomplished enzymatically.

Therefore, the enzymatic reaction product TMBox can be sensitively detected through its reduction at the surface of the PCA-RGO/Au NPs platform.

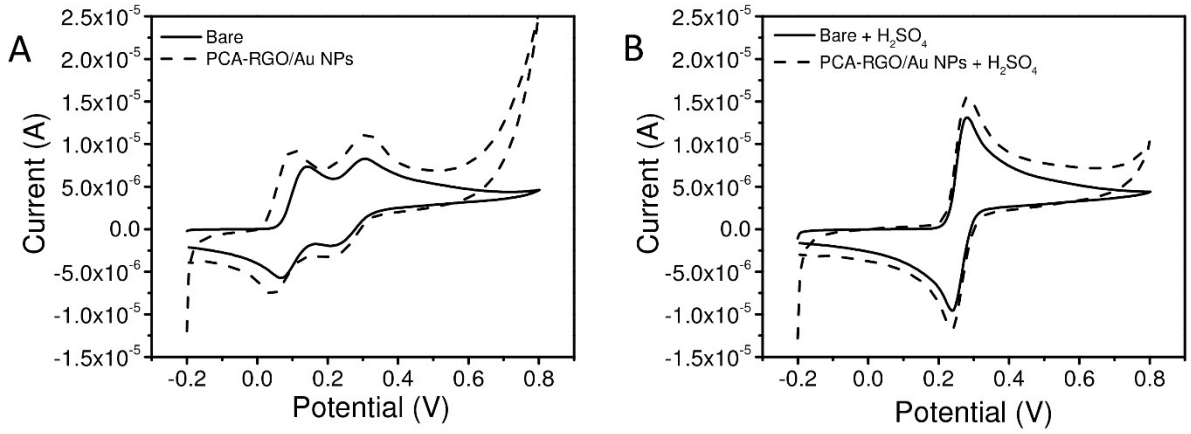

Figure S2. CVs of ready to use substrate solution containing TMB and H_2O_2, before (A) and after (B) the addition of H_2SO_4, to a final concentration of 0.5 M.

Amperometric detection of H_2O_2

Fig. S2 shows the amperometric response of SPCEs, as bare and modified by the neat PCA-RGO flakes and by the colloidal PCA-RGO/Au NPs hybrid material, at the potential of +0.65 V, to increasing levels of H_2O_2. The bare SPCEs display a slight increase of the current, in response to successive additions of H_2O_2 volumes. By contrast, the PCA-RGO/Au NPs modified SPCEs exhibit an appreciable increase of the current and the electrode reaches the 95% of the steady-state current within few seconds. Furthermore, the relative standard deviation (RSD) of the current signals related to the measurement of 0.02 mM H_2O_2, performed with five modified electrodes fabricated in parallel, is 6 %, attesting for the acceptable reproducibility of the electrode fabrication.

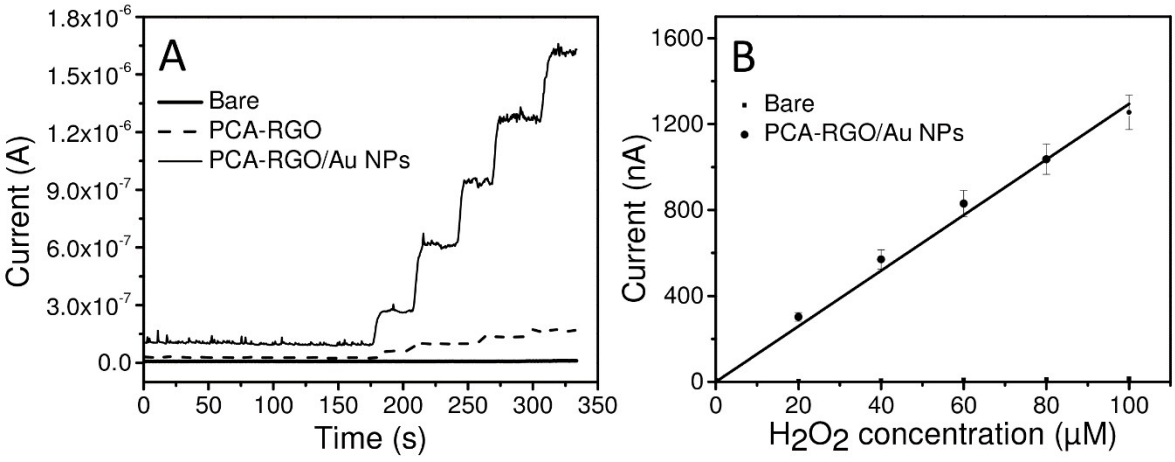

Figure S3. (A) Amperometric responses of SPCEs, as bare and modified by the PCA-RGO and PCA-RGO/Au NPs flakes, upon successive addition of a 0.02 mM H_2O_2 solution in 0.05 M PB (pH 8.5), at + 0.65 V. In (B) calibration plot of panel (A).

Spiked serum samples

Fig. S4 reports the calibration curve of miRNA-221 in spiked human blood serum samples.

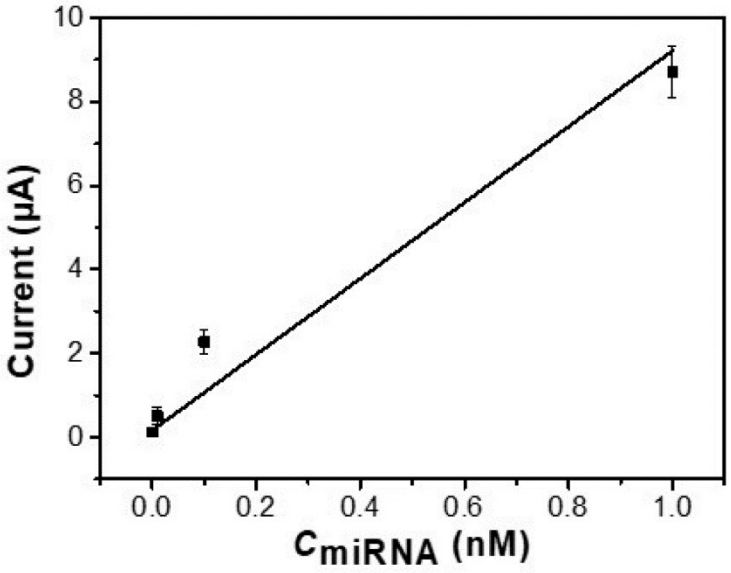

Figure S4. Calibration curve of miRNA-221 in spiked serum samples.

Table S2. Comparison of the LODs reported for some electrochemical genosensors based on Graphene-Au modified electrodes.

Electrode materials	Label	LOD	Analyte	Ref.
Graphene sheets/poly-aniline/Au NP nanocomposites	Alkaline Phosphatase	1.05 pM	BCR/ABL fusion gene	4b
Au NPs/toluidine blue–graphene oxide	---	2.95 pM	MDR1 gene	6
Graphene–mesoporous silica–Au NP hybrids	Redox mediator	6.60 pM	Synthethic DNA	13a
Three-dimensional graphene films (3DGFs) on Au substrates	HRP-mimicking DNAzyme	5.60 pM	miRNA-155	13c
Pyrene-Carboxylic Acid (PCA) surface modified RGO flakes, coated thiol-capped Au NPs	Alkaline phosphatase	0.70 pM	miRNA-221	This work

References

[1] G. Goncalves, P. A. A. P. Marques, C. M. Granadeiro, H. I. S. Nogueira, M. K. Singh and J. Gracio, Chem. Mater., 2009, 21, 4796.

[2] a) M. Rajamathi and C. Nethravathi, Carbon, 2008, 46, 1994. b) S. Li, Z. Wang, H. Jiang, L. Zhang, J. Ren, M. Zheng, L. Dong and L. Sun, Chem. Commun., 2016, 52, 10988.

[3] Q. Zhuo, Y. Ma, J. Gao, P. Zhang, Y. Xia, Y. Tian, X. Sun, J. Zhong and X. Sun, Inorg. Chem., 2013, 52, 3141

[4] H. Zhang, D. Hines and D. L. Akins, Dalton Trans., 2014, 43, 2670.

[5] C. Ingrosso, G. V. Bianco, M. Corricelli, R. Comparelli, D. Altamura, A. Agostiano, M. Striccoli, M. Losurdo, M. L. Curri, G. Bruno, ACS Appl. Mater. & Interfaces 2015, 7, 4151.

[6] L. Li, X. Zheng, J. Wang, Q. Sun and Q. Xu, ACS Sustainable Chem. Eng., 2013, 1, 144.

[7] Y.-Y. Ou and M. H. Huang, J. Phys. Chem. B, 2006, 110, 2031.

[8] L. Li, X. Zheng, J. Wang, Q. Sun and Q. Xu, ACS Sustainable Chem. Eng., 2013, 1, 144.

[9] Y.-Y. Ou, M. H. Huang, J. Phys. Chem. B, 110, 2006, 2031-2036.

[10] Fanjul-Bolado, P.; González-García, M. B.; Costa-García, A. *Anal Bioanal Chem* **2005**, *382*, 297.